

A meshfree cell-based smoothed radial point interpolation method for damage problems

Samir S. Saliba¹, Lapo Gori¹, Roque L. S. Pitangueira¹

¹*Structural Engineering Department, Federal University of Minas Gerais
Avenida Antônio Carlos, 6627, 31270-901, Belo Horizonte/MG, Brazil
samirsaliba@yahoo.com, lapo@dees.ufmg.br, roque@dees.ufmg.br*

Abstract. Meshfree methods belonging to the class of Smoothed Point Interpolation Methods (S-PIM) have been shown to provide certain advantages with respect to the standard finite element method (FEM), when dealing with physically nonlinear problems. The present work extends the Cell-Based Smoothed Radial Point Interpolation Method with polynomial reproduction (CS-RPIMp), originally proposed for linear problems, to the case of damage models. The weakened-weak (W^2) formulation and peculiar integration scheme which this method is based on have been extended to nonlinear damage models. Some numerical examples of nonlinear problems with different kinds of boundary conditions, performed using different strategies for support nodes selection based on the T-schemes (T4-, T6/3- and T2L-schemes), are presented, aiming to point out the accuracy, convergence and efficiency of the Cell-Based Smoothed Radial Point Interpolation Method with polynomial reproduction in comparison with the standard finite element method.

Keywords: Smoothed Point Interpolation Methods (S-PIMs), Cell-based (CS), Radial point interpolation method (RPIM), Meshfree methods, Scalar damage

1 Introduction

Smoothed point interpolation methods (S-PIM) are a class of methods that were developed upon a weakened-weak (W^2) formulation. This formulation endows these methods with interesting characteristics that, in general, make them more accurate than the standard FEM. Among them there are the so-called node-base smoothed point interpolation method (NS-PIM), proposed by Wu et al. [1], edge-based smoothed point interpolation method (ES-PIM), developed by Wu et al. [2], and cell-based smoothed point interpolation method (CS-PIM), presented by Liu and Zhang [3] and Zhang and Liu [4]. S-PIM methods are considered robust, efficient and simple. Simplicity can be characterized by the fact that these methods use discretized domains in triangular background cells, small numbers of nodes in the support domains and low-order interpolation functions [5].

CS-PIM models, when compared to others S-PIM models, have the advantage of making a direct use of the background cells as their smoothed domains without the need for further geometrical operations that are instead needed to build node- and edge-based domains. When used with PIM shape functions it presents some issues, that can be overcome using shape functions based on radial functions [6]. Many works based on CS-PIM models have been applied to the study of linear static problems.

This paper aims to show the use of the CS-PIM combined with the nodal selection strategies for building the support domain, T4-, T6/3- and T2L-scheme, in nonlinear damage models. For that, it was decided to investigate the numerical simulation of two experimental test available in the literature. The simulations were performed using the open-source software **INSANE**¹.

¹More informations on the project can be found at <https://www.insane.dees.ufmg.br/>; the development code is freely available at the Git repository <http://git.insane.dees.ufmg.br/insane/insane.git>.

2 Cell-based smoothed radial point interpolation method

The approximate displacement function $u(\mathbf{x})$ for a point \mathbf{x} is defined in the domain by

$$u(\mathbf{x}) = \sum_{i=1}^n \phi_i(\mathbf{x})u_i, \quad (1)$$

where n is a set of nodes, ϕ_i is the nodal shape function for the i th node and u_i is the nodal displacement at the i th node.

S-PIM methods generally use polynomial or radial basis function (RBF) in their shape functions. In the present work, the radial point interpolation method with polynomials reproduction (RPIMP), presented by Liu and Gu [7], that combines both, radial basis functions and polynomials in the basis will be used. The displacement field is approximated at a point \mathbf{x} , by

$$u(\mathbf{x}) = \sum_{i=1}^n R_i(\mathbf{x})b_i + \sum_{j=1}^m p_j(\mathbf{x})a_j = \mathbf{R}^T(\mathbf{x})\mathbf{b} + \mathbf{p}^T(\mathbf{x})\mathbf{a} = \begin{bmatrix} \mathbf{R}^T(\mathbf{x}) & \mathbf{p}^T(\mathbf{x}) \end{bmatrix} \begin{bmatrix} \mathbf{b} \\ \mathbf{a} \end{bmatrix}, \quad (2)$$

where n is a set of nodes in the neighborhood of \mathbf{x} , m is the number of polynomial base functions, b_i and a_j are coefficients associated to the RBFs and polynomials, respectively, R_i is the radial base function and p_j the monomials of the polynomial base.

The coefficients associated to the RBFs and polynomials functions, b_i and a_j , can be determined satisfying eq. (2) at the n nodes within the support domain. Thus eq. (2) can be rewritten in matrix form by

$$\begin{bmatrix} \mathbf{u} \\ \mathbf{0} \end{bmatrix} = \begin{bmatrix} \mathbf{R}_Q & \mathbf{P}_m \\ \mathbf{P}_m & \mathbf{0} \end{bmatrix} \begin{bmatrix} \mathbf{b} \\ \mathbf{a} \end{bmatrix} = \mathbf{G} \begin{bmatrix} \mathbf{b} \\ \mathbf{a} \end{bmatrix}, \quad (3)$$

where \mathbf{G} is the combined moment matrix composed by

$$\mathbf{R}_Q = \begin{bmatrix} R_1(r_1) & R_2(r_1) & \dots & R_n(r_1) \\ R_1(r_2) & R_2(r_2) & \dots & R_n(r_2) \\ \vdots & \vdots & \ddots & \vdots \\ R_1(r_n) & R_2(r_n) & \dots & R_n(r_n) \end{bmatrix}, \quad \mathbf{P}_m = \begin{bmatrix} P_1(\mathbf{x}_1) & P_2(\mathbf{x}_1) & \dots & P_m(\mathbf{x}_1) \\ P_1(\mathbf{x}_2) & P_2(\mathbf{x}_2) & \dots & P_m(\mathbf{x}_2) \\ \vdots & \vdots & \ddots & \vdots \\ P_1(\mathbf{x}_n) & P_2(\mathbf{x}_n) & \dots & P_m(\mathbf{x}_n) \end{bmatrix}. \quad (4)$$

Manipulating eq. (3) and replacing it in eq. (2), the approximation of displacement field can be rewritten as follows

$$u(\mathbf{x}) = \begin{bmatrix} \mathbf{R}^T(\mathbf{x}) & \mathbf{p}^T(\mathbf{x}) \end{bmatrix} \mathbf{G}^{-1} \begin{bmatrix} \mathbf{u} \\ \mathbf{0} \end{bmatrix}, \quad (5)$$

where the shape functions is given by

$$\phi(\mathbf{x}) = \begin{bmatrix} \mathbf{R}^T(\mathbf{x}) & \mathbf{p}^T(\mathbf{x}) \end{bmatrix} \mathbf{G}^{-1}. \quad (6)$$

RPIMP shape functions satisfy the Kronecker delta property, that is an important feature because it allows a straightforward imposition of boundary conditions.

2.1 T-schemes for nodes selection

The same background mesh used to build the smoothing domains can also be used to select the nodes in the support domain that will be used to build the shape functions.

Due to the ease of creation in addition to other important aspects, generally triangular type background meshes are used to discretize the domain, thus allowing the use of the so-called T-schemes. This nodal selection strategy is based on the triangular cell where the point of interest is located.

According to Liu and Zhang [5, 8], T-schemes have been found to be most practical, robust, efficient and works well for the S-PIM models. Among the various existing schemes, the following will be used in this work: T4-, T6/3- and T2L-scheme.

2.2 Construction of the Smoothing Domains

The S-PIM models use so-called smoothed strain fields in their formulation. These smoothed strain fields provide unique, important and attractive features to these models.

The construction of these strain fields is based on a set of smoothing domains, where the strain is assumed to be uniform. These smoothing domains are a tessellation of the problem domain into subdomains that must cover it without overlaps or gaps [3]. The way these smoothing domains will be formed and their quantity, is related to the specific S-PIM model, and can be based on a node, edge or face (cell) of the background mesh.

The cell-based strategy has its smoothing domains based on faces (cells). In this way, since the problem domain is already discretized by a triangular background mesh, each triangle of this mesh becomes a smoothing domain, thus avoiding further geometrical operations that are instead needed to generate node- and edge-based smoothing domains. The points of interest or integration points are located on the edges of each triangle, as pointed out in Fig. 1.

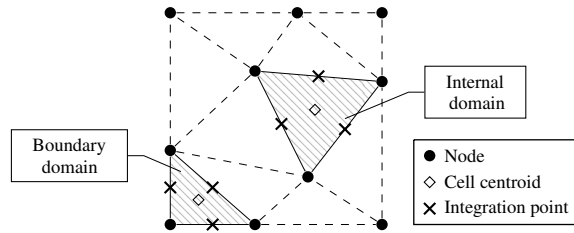


Figure 1. Cell-base smoothing domain

3 Constitutive model

The behaviour of quasi-brittle materials during a loading-unloading process can be described with elastic-degrading models, where the material elastic properties progressively degrades as the strains exceed certain threshold values.

A feature of these models is the existence of a total relationship between stresses and strains, which can be expressed by

$$\boldsymbol{\sigma} = \hat{\mathbf{E}}^S \boldsymbol{\varepsilon}, \quad \boldsymbol{\varepsilon} = (\hat{\mathbf{E}}^S)^{-1} \boldsymbol{\sigma}, \quad (7)$$

where $\boldsymbol{\sigma}$ is the stress tensor, $\boldsymbol{\varepsilon}$ is the strain tensor and $\hat{\mathbf{E}}^S$ is the secant constitutive operator. Disregarding the micro cracks closure-reopening effects, the secant operator remains constant within an unloading-reloading process.

3.1 Scalar damage

Scalar damage models are the most simple ones among the different elastic-degrading models. Their secant constitutive operator is expressed as [9–11]

$$\hat{\mathbf{E}}^S(D, \hat{\mathbf{E}}^0) = (1 - D) \hat{\mathbf{E}}^0, \quad (8)$$

where D is a scalar damage variable, assumed to vary from 0 (undamaged material) to 1 (completely damaged material), and $\hat{\mathbf{E}}^0$ is the initial constitutive operator.

For a scalar damage model, a common choice for the loading function is represented by the following additive decomposition

$$f(\boldsymbol{\varepsilon}, D) = \varepsilon_{eq}(\boldsymbol{\varepsilon}) - K(D) \leq 0, \quad (9)$$

where $\varepsilon_{eq}(\boldsymbol{\varepsilon})$ is an equivalent strain, and $K(D)$ is a historical parameter that is representative of the maximum level of strain reached during the loading process. The damage variable is usually prescribed as a function of the equivalent strain; in this work the following exponential damage law is being adopted

$$D(\varepsilon_{eq}) = 1 - \frac{K_0}{\varepsilon_{eq}} (1 - \alpha + \alpha e^{-\beta(\varepsilon_{eq} - K_0)}), \quad (10)$$

where K_0 is a threshold value for the equivalent strain, α and β are parameters that define the maximum allowed damage level and the damage evolution intensity, respectively. In this work, the Mazars scalar damage model [12, 13] was applied, and the equivalent deformation is given by

$$\varepsilon_{eq} = \sqrt{\left[\sum_{k=1}^3 (\langle \varepsilon^{(k)} \rangle_+)^2 \right]}, \quad (11)$$

where $\varepsilon^{(k)}$ is the k th eigenvalue of the strain tensor and $\langle \varepsilon^{(k)} \rangle_+ = (\varepsilon^{(k)} + |\varepsilon^{(k)}|)/2$ its positive part.

4 Numerical simulations

In this section, two numerical simulations are presented using the CS-RPIMp strategy in physically nonlinear analyses. To compare the performance of this meshfree method, the results obtained with three nodal selection strategies, T4-, T6/3- and T2L-schemes, are compared with the results obtained by FEM models using triangular elements with three nodes, and also with results of experimental tests.

4.1 L-shaped panel

The L-shaped panel illustrated in Fig. 2a has a thickness equal to 100 mm and is subjected to a vertical force $F = 7000$ N. The material parameters experimentally obtained by Winkler et al. [14] and adopted in the numerical simulation are: Young's modulus $E = 25850$ MPa, Poisson's ratio $\nu = 0.18$, tensile strength $f_t = 2.7$ MPa, compressive strength $f_c = 4.0$ MPa, fracture energy $G_f = 0.065$ MPa and a characteristic length $h = 28.0$ mm. The Mazars scalar damage model was adopted with the following parameters for the exponential damage law (eq. (10)): $\alpha = 0.95$, $\beta = 1100$ and $K_0 = 1.12 \times 10^{-4}$.

The Newton-Raphson method was applied with the displacement control method to solve the system of nonlinear equations, for that a vertical displacement increment equal to 7.5×10^{-4} mm was applied at the node of load application, and a tolerance for the convergence in displacement of 1×10^{-4} .

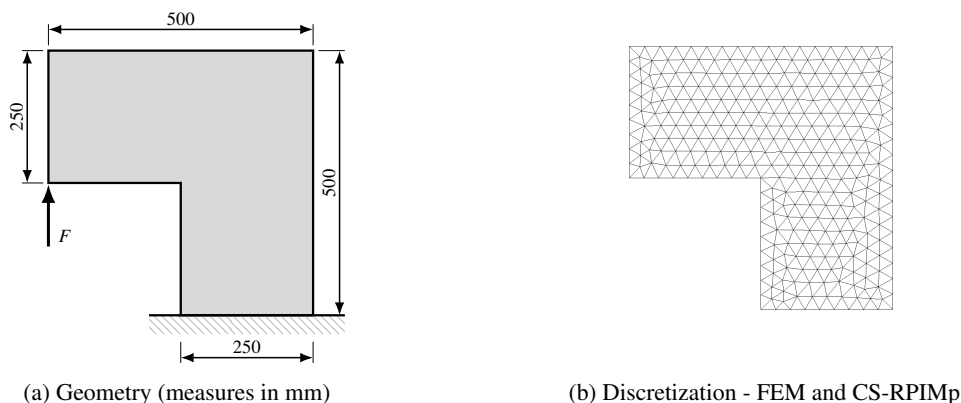


Figure 2. L-shaped panel

The meshfree shape functions were constructed with the radial point interpolation method with polynomials reproduction, using the exponential radial function with $c = 0.002$ and 3 polynomial terms. The tangent approximation of the constitutive operator was considered to perform these simulations.

The equilibrium paths were obtained from the vertical displacement of the point where the load is applied. Experimental results were reproduced from Winkler et al. [14].

The results shown in Fig. 3 point out that CS-RPIMp with T4-scheme was the configuration that best described the global response of the structure. For the softening branch, the T4 and T6/3 strategies were able to describe the behaviour well. Finally, T4- and T6/3-scheme again showed greater precision in the limit load value.

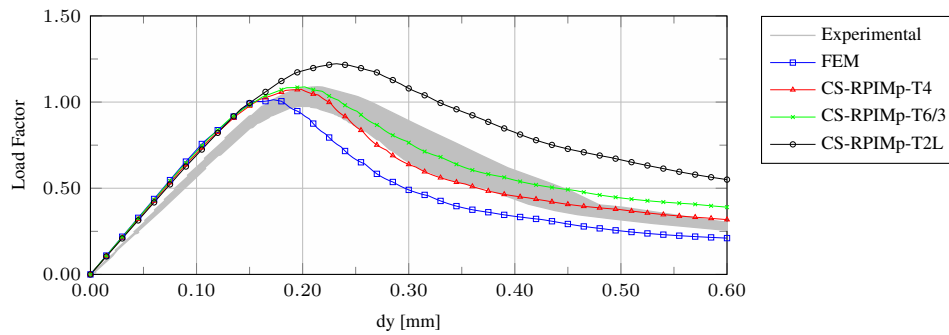


Figure 3. L-shaped panel - Equilibrium paths

4.2 Three-point bending test

The beam illustrated in Fig. 4a has a thickness equal to 50 mm and it is subjected to a vertical force $F = 800$ N. For the numerical simulation, the following material parameters experimentally obtained by Petersson [15] were used: Young's modulus $E = 30000$ MPa, Poisson's ratio $\nu = 0.2$, tensile strength $f_t = 3.33$ MPa, compressive strength $f_c = 33.3$ MPa and fracture energy $G_f = 0.124$ MPa. The Mazars scalar damage model was adopted with the following parameters for the exponential damage law (eq. (10)): $\alpha = 0.95$, $\beta = 1100$ and $K_0 = 1.10 \times 10^{-4}$.

The solution of the system of nonlinear equations was performed using the Newton-Raphson method with the displacement control strategy, using the force application node as the control point, and vertical displacement increment of -5.0×10^{-3} mm. The tolerance considered for convergence was 1×10^{-4} .

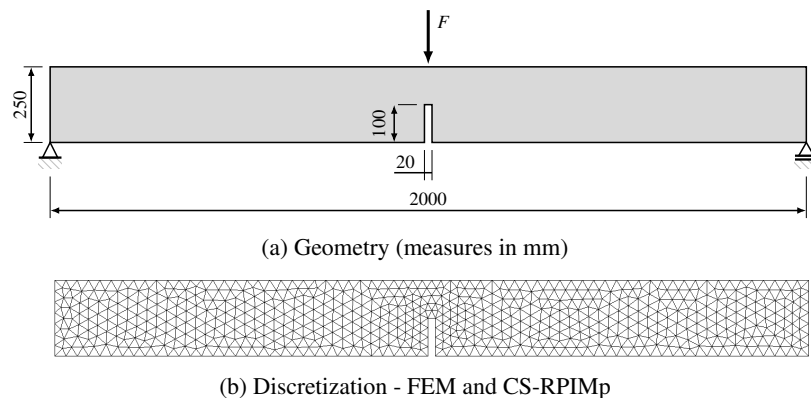


Figure 4. Three-point bending

The meshfree shape functions were constructed with the radial point interpolation method with polynomials reproduction, using the exponential radial function with $c = 0.002$ and 3 polynomial terms. The tangent approximation of the constitutive operator was considered to perform the simulations.

The equilibrium path was described for the vertical displacement of the point where the load is applied. Experimental results were reproduced from Petersson [15].

As can be seen in Fig. 5 the elastic branch was very well represented by all models, the softening branch was best represented by CS-RPIMp with T6/3-scheme, this being the model that best reproduced the physical test. A highlight of this simulation was the almost identical behaviour of the FEM and CS-RPIMp with T4-scheme, different from what happened in the simulation presented in section 4.1. The T2L-scheme after the linear part of the equilibrium path, it started to distance itself from the experimental test and for numerical reasons it stopped before the end of the number of steps established in this analysis. Once again, T4- and T6/3-scheme showed good values of limit load, in addition to good behaviour throughout the analysis.

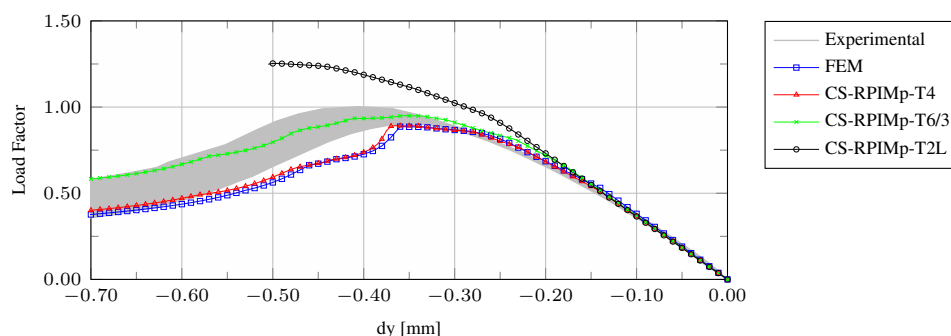


Figure 5. Three point bending - Equilibrium paths

5 Conclusions

In the present work it was presented the use of the cell-based smoothed point interpolation method in the study of physically nonlinear problems. A comparison between three different nodal selection strategies for the construction of the support domain were applied in the two numerical simulations, in addition to comparing the results obtained through this meshfree method with the finite element method and the experimental test. In the two simulations performed, the CS-RPIMp with T4- and T6/3-scheme obtained equilibrium paths similar to the experimental test, however the T2L-scheme, which uses a much larger number of nodes in the support domain, presented good results only in the elastic branch. It is also possible to observe that in both simulations, the addition of nodes in the support domain made CS-RPIMp a little more rigid in the softening branch. In general, the main aim of the work can be demonstrated, in addition to opening possibilities for further research on the topic.

Acknowledgements. The authors gratefully acknowledge the support from the Brazilian research agencies CAPES (Coordenação de Aperfeiçoamento de Pessoal de Nível Superior), FAPEMIG (Fundação de Amparo à Pesquisa do Estado de Minas Gerais; grant PPM-00747-18), and CNPq (Conselho Nacional de Desenvolvimento Científico e Tecnológico; grant 309515/2017-3).

Authorship statement. The authors hereby confirm that they are the sole liable persons responsible for the authorship of this work, and that all material that has been herein included as part of the present paper is either the property (and authorship) of the authors, or has the permission of the owners to be included here.

References

- [1] Wu, S. C., Liu, G. R., Zhang, H. O., & Zhang, G. Y., 2009. A node-based smoothed point interpolation method (NS-PIM) for thermoelastic problems with solution bounds. *International Journal of Heat and Mass Transfer*, vol. 52, pp. 1464–1471.
- [2] Wu, S. C., Liu, G., Cui, X. Y., Nguyen, T., & Zhang, G. Y., 2010. An edge-based smoothed point interpolation method (ES-PIM) for heat transfer analysis of rapid manufacturing system. *International Journal of Heat and Mass Transfer*, vol. 53, pp. 1938–1950.
- [3] Liu, G. R. & Zhang, G. Y., 2009. A normed G space and weakened weak (W^2) formulation of a cell-based smoothed point interpolation method. *International Journal of Computational Methods*, vol. 6(1), pp. 147–179.
- [4] Zhang, G. & Liu, G. R., 2010. A meshfree cell-based smoothed point interpolation method for solid mechanics problems. In *AIP Conference Proceedings*, volume 1233, pp. 887–92, Hong Kong, Macau (China). AIP.
- [5] Liu, G. R. & Zhang, G. Y., 2013. *Smoothed point interpolation methods: G space theory and weakened weak forms*. World Scientific Publishing Co. Pte. Ltd.
- [6] Zhang, G. Y. & Liu, G. R., 2011. Meshfree cell-based smoothed point interpolation method using isoparametric PIM shape functions and condensed RPIM shape functions. *International Journal of Computational Methods*, vol. 8(4), pp. 705–730.
- [7] Liu, G. R. & Gu, Y. T., 2001. A local radial point interpolation method (LRPIM) for free vibration analyses of 2-D solids. *Journal of Sound and Vibration*, vol. 246(1), pp. 29–46.
- [8] Liu, G. R., 2009. *Meshfree methods: Moving beyond the finite element method*. CRC Press, 2nd edition.
- [9] Carol, I., Rizzi, E., & Willam, K., 1994. A unified theory of elastic degradation and damage based on a loading surface. *International Journal of Solids and Structures*, vol. 31, pp. 2835–2865.

- [10] Penna, S. S., 2011. *Formulação Multipotencial para Modelos de Degradação Elástica: Unificação Teórica, Proposta de Novo Modelo, Implementação Computacional e Modelagem de Estruturas de Concreto*. PhD thesis, Escola de Engenharia de Estruturas da Universidade Federal de Minas Gerais, Belo Horizonte, Brazil.
- [11] Gori, L., Penna, S. S., & Pitangueira, R. L. S., 2017. A computational framework for constitutive modelling. *Computers and Structures*, vol. 187, pp. 1–23.
- [12] Mazars, J., 1984. *Application de la Mécanique de l'endommagement au comportement non linéaire et à la rupture du béton de Structure*. PhD thesis, Université Pierre et Marie Curie - Laboratoire de Mécanique et Technologie, Paris, France (in french).
- [13] de Borst, R. & Gutiérrez, M. A., 1999. A unified framework for concrete damage and fracture models including size effects. *International Journal of Fracture*, vol. 95, pp. 261–277.
- [14] Winkler, B., Hofstetter, G., & Lehar, H., 2004. Application of a constitutive model for concrete to the analysis of a precast segmental tunnel lining. *International Journal for Numerical and Analytical Methods in Geomechanics*, vol. 28, pp. 797–819.
- [15] Petersson, P., 1981. Crack growth and development of fracture zones in plain concrete and similar materials. In *Tech. Rep. TVBM-1006, Division of Building Materials*, Lund (Sweden). Lund Institute of Technology.